Eur. Phys. J. A (2016) **52**: 195
DOI 10.1140/epja/i2016-16195-9

THE EUROPEAN PHYSICAL JOURNAL A

Regular Article – Experimental Physics

Photo-neutron reaction cross-sections for ^{nat}Mo in the bremsstrahlung end-point energies of 12–16 and 45–70 MeV

H. Naik[1,a], G.N. Kim[2], R. Kapote Noy[3], R. Schwengner[4], K. Kim[2], M. Zaman[2], S.G. Shin[5], Y. Gey[5], R. Massarczyk[4], R. John[4], A. Junghans[4], A. Wagner[4], and M.-H. Cho[5]

[1] Radiochemistry Division, Bhabha Atomic Research Centre, Mumbai 400085, India
[2] Department of Physics, Kyungpook National University, Daegu 702-701, Republic of Korea
[3] Division of Physical and Chemical Sciences, Department of Nuclear Sciences and applications, IAEA, Vienna International Centre, P.O. Box 100, A-1400 Vienna, Austria
[4] Institute of Radiation Physics, Helmholtz-Zentrum Dresden-Rossendorf, 01328 Dresden, Germany
[5] Division of Advanced Nuclear Engineering, Pohang University of Science and Technology, Pohang 790-784, Republic of Korea

Received: 27 March 2016 / Revised: 30 May 2016
Published online: 21 July 2016 –
Communicated by R.K. Bhandari

Abstract. The ^{nat}Mo$(\gamma, x\mathrm{n})^{90,91,99}$Mo reaction cross-sections were experimentally determined for the bremsstrahlung end-point energies of 12, 14, 16, 45, 50, 55, 60 and 70 MeV by activation and off-line γ-ray spectrometric technique and using the 20 MeV electron linac (ELBE) at the Helmholtz-Zentrum Dresden-Rossendorf (HZDR), Dresden, Germany, and the 100 MeV electron linac at the Pohang Accelerator Laboratory (PAL), Pohang, Korea. The ^{nat}Mo$(\gamma, x\mathrm{n})^{88,89,90,91,99}$Mo reaction cross-sections as a function of photon energy were also calculated using the computer code TALYS 1.6. The flux-weighted average cross-sections were obtained from the literature data and the calculated values of TALYS based on mono-energetic photons and are found to be in general agreement with the present results. The flux-weighted average experimental and theoretical cross-sections for the ^{nat}Mo$(\gamma, x\mathrm{n})^{88,89,90,91,99}$Mo reactions increase with the bremsstrahlung end-point energy, which indicates the role of excitation energy. After a certain energy, the individual ^{nat}Mo$(\gamma, x\mathrm{n})$ reaction cross-sections decrease with the increase of bremsstrahlung energy due to opening of other reactions, which indicates sharing of energy in different reaction channels. The ^{100}Mo(γ, n) reaction cross-section is important for the production of ^{99}Mo, which is a probable alternative to the ^{98}Mo(n, γ) and ^{235}U(n, f) reactions.

1 Introduction

Nuclear reaction cross-sections of various materials are important for the study of the nuclear structure and reactions mechanisms. In particular, the photon- and neutron-induced cross-sections of various materials in a wide range of energies are important for different applications such as the design of radiation shielding, the calculation of absorbed dose in the human body during radiotherapy, in the physics and technology of fusion and fission reactors, nuclear waste estimation and transmutation and astrophysical nucleo-synthesis [1,2]. Besides this, the nuclear reaction cross-sections related to the radioactive isotopes are necessary for their productions and to test the theoretical model. This is because radioactive isotopes are widely used in industry, medicine and the life sciences [3,4]. About 140 radioisotopes are used worldwide in medical application such as therapeutic, preventive and non-invasive nuclear diagnostic imaging techniques [5–14]. Among the medical radioisotopes, ^{99m}Tc is utilized in 80% of all nuclear medicine studies [15–20]. ^{99m}Tc has a half-life of 6.0 h and produced by milking out from the parent ^{99}Mo having half-life of 65.94 h [21–24].

Natural Mo is used as a target for the production of medical radio-isotopes such as ^{99}Mo-^{99m}Tc, ^{96}Tc, ^{94m}Tc, etc., by using different nuclear reactions. In research reactor, high specific activity of ^{99}Mo is produced from the ^{235}U$(\mathrm{n}, \mathrm{f})^{99}$Mo reaction. About 90% of ^{99}Mo used in the world is produced in reactor from ^{235}U$(\mathrm{n_{th}}, \mathrm{f})$ reaction using highly enriched (93%) uranium (HEU) and 10% from ^{98}Mo$(\mathrm{n_{th}}, \gamma)$ reaction. In the ^{235}U$(\mathrm{n}, \mathrm{f})^{99}$Mo reaction, many long-lived radioactive wastes with total activity of fifty times the activity of ^{99}Mo are formed [25–27]. To avoid the radioactive waste, required ^{99}Mo activity can be obtained from the ^{98}Mo$(\mathrm{n_{th}}, \gamma)$ reaction by using enriched ^{98}Mo target and high flux reactor. It is also possible to produce the activity of ^{99}Mo from the ^{100}Mo$(\mathrm{n}, 2\mathrm{n})^{99}$Mo reaction [28–30]. In the high-energy neutron-induced reaction, other reaction products also produce along with ^{99}Mo. Besides this, generating sufficient high-energy neutron flux

[a] e-mail: naikhbarc@yahoo.com (corresponding author)

with proper shielding and hazardless biological effect is not easy to achieve. The activity of ^{99}Mo and its daughter product ^{99m}Tc can be produced from the ^{100}Mo(p, pn) and ^{100}Mo(p, 2n) reactions [31–42]. In the proton-induced reactions of natural molybdenum, many radioactive products with high specific activities are produced. This is because ^{nat}Mo has the isotopic composition of ^{92}Mo (14.84%), ^{94}Mo (9.25%), ^{95}Mo (15.92%), ^{96}Mo (16.68%), ^{97}Mo (9.55%), ^{98}Mo (24.13%) and ^{100}Mo (9.63%), respectively. As a probable alternative to the above reactions, ^{99}Mo-^{99m}Tc can be obtained by the ^{100}Mo$(\gamma, n)^{99}$Mo reaction [43–47]. Since the ^{nat}Mo has so many isotopes, their (γ, x) reactions at higher photon energy produce $^{91\text{-}88}$Mo and other radioactive nuclides such as $^{90\text{-}97}$Nb and $^{86\text{-}89}$Zr besides ^{99}Mo [47–49]. The mono-energetic photon with sufficient flux is difficult to obtain. Thus production of useable activity of ^{99}Mo from ^{100}Mo(γ, n) reaction with mono-energetic photon is a difficult task. Nowadays most of the photo-nuclear reactions studies have been made by the use of bremsstrahlung from electron accelerators. Owing to the development of accelerator technology, there is the feasibility of ^{99}Mo production from the ^{100}Mo(γ, n) reaction as an alternative to the ^{98}Mo(n_{th}, γ) reaction. This is because the ^{100}Mo$(\gamma, n)^{99}$Mo reaction has higher cross-section of 152.3 mb at the photon energy of 14.56 MeV [47] compared to the ^{98}Mo$(n_{th}, \gamma)^{99}$Mo reaction cross-section of 130 mb [50]. In ^{nat}Mo, the isotopic abundance of ^{100}Mo is 9.63%, whereas for ^{98}Mo, it is 24.13%. The production of ^{99}Mo activity from the (γ, n) reaction of ^{100}Mo and ^{nat}Mo at different bremsstrahlung end-point energies has been shown by us [51] and others [6,17]. The ^{100}Mo(γ, n) cross-section at the bremsstrahlung end-point energies of 10 and 12.5 MeV was also determined by us [52]. At the bremsstrahlung end-point energies of 10 and 12.5 MeV, only ^{100}Mo(γ, n) and ^{92}Mo$(\gamma, n)^{91}$Mo reactions can take place in the ^{nat}Mo target. The relative ^{nat}Mo$(\gamma, xn)^{91m,g}$Mo reaction cross-section has been recently published by us [53] at the bremsstrahlung end-point energies of 12–16 and 45–70 MeV. Other than our data [52,53], no cross-sections data for the ^{100}Mo(γ, n) or ^{nat}Mo(γ, xn) reactions induced by bremsstrahlung are available in the literature. In the present work, we have measured the cross-sections for the ^{nat}Mo$(\gamma, xn)^{90,91,99}$Mo reactions at the bremsstrahlung end-point energies of 12–16 and 45–70 MeV by using activation and off-line γ-ray spectrometry technique. The relative ^{nat}Mo$(\gamma, xn)^{91m,g}$Mo reaction cross-section from ref. [53] has also been updated in the present work. The ^{nat}Mo$(\gamma, xn)^{88\text{-}91,99}$Mo reaction cross-section induced by 12–16 and 45–70 MeV bremsstrahlung was calculated theoretically by using the computer code TALYS 1.6 [54] and compared with the experimental data.

2 Experimental details

The experiments for the measurement of ^{nat}Mo$(\gamma, x)^{91,99}$Mo reaction cross-sections at the end-point bremsstrahlung energy of 12, 14 and 16 MeV were done by using the 20 MeV electron linac (ELBE) at HZDR, Germany. For each irradiation, a stack of the ^{nat}Mo-Au sample was made. The size of the 99.999% pure ^{nat}Mo metal foil was 1 cm × 0.6–0.8 cm with thickness of 0.1 mm and weight 54.80.4 mg. On the other hand, the size of the Au metal foil was 0.8 cm × 0.7–0.6 cm with thickness of 0.1 mm and weight 83.2–101.6 mg. The ^{197}Au$(\gamma, n)^{196}$Au reaction was used as the photon flux monitor. The samples were wrapped with 0.025 mm thick aluminium foil with purity more than 99.99%. The metal samples were kept separately inside three different capsules made of polypropylene and loaded on a sample holder. They were sent to the irradiation site one at a time using pneumatic carrier rabbit facility [55,56]. The bremsstrahlung was generated by impinging the electron beam on a solid graphite beam dump [55,56]. The area directly behind the electron beam dump was used as a site for high flux ($\sim 10^9$ to 10^{10} photons cm^{-2} s^{-1}) irradiations. The samples were irradiated for 8.5 to 10.5 hours with the end-point bremsstrahlung energy of 12–16 MeV. During the experiments, the electron LINAC was operated with a pulse repetition rate (PRR) of 13 MHz, a pulse width of 10 picoseconds and an average beam current of 550 μA. The electron beam current was stable and thus produces constant photon flux throughout the irradiation. After the irradiation, the samples were brought back to the detector by using the same automated pneumatic rabbit carrier facility. The γ-ray counting of the irradiated targets of ^{nat}Mo and Au along with individual Al wrapper was done separately by using energy and efficiency-calibrated 90% HPGe detector coupled to a PC-based 16 K channel analyzer. The resolution of the detector system was 2.0 keV at 1332.0 keV of ^{60}Co. The sample was kept at a suitable distance from the detector to minimize the loss of counts. At the same time the dead time of the detector system was kept below 10% to avoid the coincidence and summing effects. The energy and efficiency calibration of the detector system was done by counting the γ-ray energies of standard sources such as ^{133}Ba, ^{137}Cs, ^{22}Na and ^{60}Co. Typical γ-ray spectrum of the irradiated ^{197}Au sample along with ^{27}Al wrapper from the irradiation of the bremsstrahlung end-point energy of 16 MeV from ELBE electron linac is shown in fig. 1.

The experiments for the measurement of ^{nat}Mo$(\gamma, xn)^{90,91,99}$Mo reaction cross-sections at the bremsstrahlung end-point energies of 45, 50, 55, 60, and 70 MeV were done by using the 100 MeV electron linac at Pohang accelerator laboratory (PAL), Korea. The bremsstrahlung was generated when a pulsed electron beam hit a thin tungsten (W) foil with a size of 10.0 cm × 10.0 cm and a thickness of 0.1 mm [57]. The W target was placed on a suitable stand at a distance of 18.0 cm from the electron beam exit window. The ^{nat}Mo foil with an area of 1.0 cm × 1.0 cm and weight 109.3 to 119.2 mg was wrapped with 0.025 mm thick Al foil. Similarly, the Au metal foil of same size was also wrapped with 0.025 mm thick Al foil. The Al wrapper is necessary to stop reaction products recoiling out from the target during irradiation and to avoid radioactive contamination to the surrounding. Then a stack of ^{nat}Mo-Au sample was

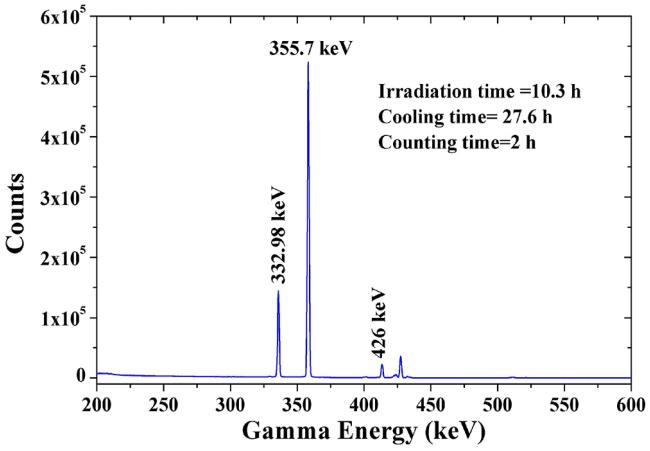

Fig. 1. Typical γ-ray spectrum of an irradiated gold foil with the bremsstrahlung end-point energy of 16 MeV.

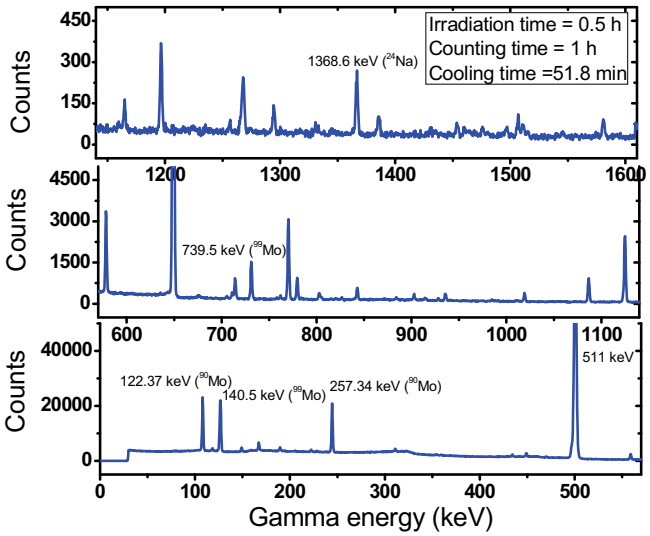

Fig. 2. Typical γ-ray spectrum of an irradiated ^{nat}Mo along with ^{27}Al wrapper with the bremsstrahlung end-point energy of 45 MeV showing the γ-lines of ^{99}Mo and ^{90}Mo from the ^{nat}Mo$(\gamma, x\mathrm{n})$ reaction and ^{24}Na from the ^{27}Al$(\gamma, 2\mathrm{pn})$ reaction, respectively.

made and additionally wrapped with one more Al foil. The ^{197}Au$(\gamma, \mathrm{n})^{196}$Au reaction cross-section was used as the photon flux monitor for the ^{100}Mo$(\gamma, \mathrm{n})^{99}$Mo reaction. On the other hand, the ^{27}Al$(\gamma, 2\mathrm{pn})^{24}$Na reaction of the Al wrapper was used to determine the photon flux for the ^{nat}Mo$(\gamma, x\mathrm{n})^{91}$Mo, and ^{nat}Mo$(\gamma, x\mathrm{n})^{90}$Mo reactions. The uses of different photon flux monitors for various reactions are based on their threshold values. The assembled sample stack was placed at a distance of 12 cm from the W target and was positioned at zero degree with respect to the direction of the electron beam [57]. Different sets of ^{nat}Mo-Au targets stack were made for different irradiations. The assembled sample was irradiated for 20–30 min with bremsstrahlung produced by bombarding the 45–70 MeV electrons on the tungsten metal foil. The current of the electron beam during irradiation was 10–35 mA at 3.75 Hz with a pulse width of 1.5 μs. The electron beam current was stable during the irradiation time. During the irradiation, some electrons also produce or pass through the thin tungsten metal foil along with the bremsstrahlung. Within the Weizsacker-Williams approximation [58,59], the electron-nucleus interaction occurs through a spectrum of virtual photons, while the bremsstrahlung is composed of real photons. Thus, the photo-nuclear reactions at the high-energy electron beam are due to the spectrum of bremsstrahlung and virtual photons. After the irradiation, the irradiated target was taken out immediately within 1–2 min for γ-ray counting. The targets of ^{nat}Mo and Au along with individual Al wrapper were taken out from the irradiated assembly and mounted separately on different Perspex (acrylic glass, 1.5 mm thick) plate [57]. The γ-ray counting of the reaction products from ^{nat}Mo, ^{197}Au and ^{27}Al were done by using an energy- and efficiency-calibrated HPGe detector coupled to a PC-based 4 K-channel analyzer. The resolution of the detector system had a full width at half maximum (FWHM) of 1.8 keV at the 1332.5 keV peak of ^{60}Co. The standard source used for the energy and the efficiency calibration was ^{152}Eu, having γ-rays in the energy range of 121.8–1408.0 keV. The detector efficiency was 20% at 1332.5 keV relative to a 3″ diameter $\times$3″ length NaI(Tl) detector. The dead time of the detector system during counting was always kept less than 10% to avoid pileup effect. The γ-ray counting of the reaction products from the irradiated samples of ^{nat}Mo, ^{197}Au and ^{27}Al were done by placing the samples in the shelf, which was 5 cm away from the detector. The γ-ray counting of the sample was done in live time mode and was followed as a function of time for at least three half-lives. Typical γ-ray spectrum of the irradiated ^{nat}Mo samples along with ^{27}Al wrapper from the irradiation of the bremsstrahlung end-point energies of 45 MeV from PAL electron linac is given in fig. 2.

3 Data analysis

3.1 Calculation of photon flux

In the case of 12–16 MeV bremsstrahlung irradiation, the photon flux was determined by using the ^{197}Au$(\gamma, \mathrm{n})^{196}$Au reaction monitor. On the other hand, in the case of 45–70 MeV bremsstrahlung irradiation, the photon flux was determined by using both the ^{197}Au$(\gamma, \mathrm{n})^{196}$Au and ^{27}Al$(\gamma, 2\mathrm{pn})$ reactions monitors. The net photo-peak activities (A_{net}) for the 332.98, 355.7 and 426.0 keV γ-rays of ^{196}Au as well as for the 1368.6 keV γ-ray of ^{24}Na were obtained from the total photo-peak areas after subtracting the linear Compton background. The photo-peak activities (A_{net}) for the γ-rays of ^{196}Au and ^{24}Na are related to the photon flux (φ) by the equation [51,57]

$$A_{(\mathrm{net})}\left(\frac{CL}{LT}\right) = \frac{n\langle\sigma\rangle\Phi a\varepsilon(1-e^{-\lambda t})(e^{-\lambda T})(1-e^{-\lambda CL})}{\lambda}, \quad (1)$$

Table 1. Nuclear spectroscopic data of the radio-nuclides from the ^{197}Au$(\gamma,\mathrm{n})^{196}$Au, ^{27}Al$(\gamma,2\mathrm{pn})^{24}$Na, ^{100}Mo$(\gamma,\mathrm{n})^{99}$Mo, $^{\mathrm{nat}}$Mo$(\gamma,x\mathrm{n})^{91\mathrm{m,g}}$Mo, $^{\mathrm{nat}}$Mo$(\gamma,x\mathrm{n})^{90}$Mo, $^{\mathrm{nat}}$Mo$(\gamma,x\mathrm{n})^{89}$Mo and $^{\mathrm{nat}}$Mo$(\gamma,x\mathrm{n})^{88}$Mo reactions [21–24]. The γ-ray energies marked with bold are used in the calculation.

Nuclide	Half-life	Decay mode (%)	γ-ray energy (keV)	γ-ray abundance (%)	Reactions	Q-value (MeV)	Threshold (MeV)
^{196}Au	6.183 d	β^+ (92.8) β^- (7.2)	332.98 **355.69** 426.0	22.9 87 7	^{197}Au(γ,n)	−8.072	8.073
^{24}Na	14.959 h	β^- (100)	**1368.6** 2754.03	100 99.944	^{27}Al$(\gamma,2\mathrm{pn})$	−31.428	31.447
^{99}Mo	65.94 h	β^- (100)	**140.5** **739.5**	89.43 12.13	^{100}Mo(γ,n)	−8.292	8.292
$^{91\mathrm{m}}$Mo	65 s	β^+ (49.9) IT (50.1)	**652.9** **1208.09** **1507.9**	48 18.7 24.3	^{92}Mo(γ,n) ^{94}Mo$(\gamma,3\mathrm{n})$ ^{95}Mo$(\gamma,4\mathrm{n})$	−12.670 −30.413 −37.787	12.671 30.423 37.795
$^{91\mathrm{g}}$Mo	15.49 min	β^+ (100)	**1581.04**	0.226	^{96}Mo$(\gamma,5\mathrm{n})$	−46.942	46.954
^{90}Mo	5.56 h	β^+ (100)	**122.37** **257.34**	64.2 78.3	^{92}Mo$(\gamma,2\mathrm{n})$ ^{94}Mo$(\gamma,4\mathrm{n})$ ^{95}Mo$(\gamma,5\mathrm{n})$ ^{96}Mo$(\gamma,6\mathrm{n})$	−22.778 −40.525 −47.894 −57.049	22.781 40.535 47.907 57.067
^{89}Mo	2.04 min	β^+ (100)	658.6 844.0 1272.6	5.7 3.7 3.7	^{92}Mo$(\gamma,3\mathrm{n})$ ^{94}Mo$(\gamma,5\mathrm{n})$ ^{96}Mo$(\gamma,6\mathrm{n})$	−36.009 −53.755 −61.124	36.014 53.771 61.145
^{88}Mo	8.0 min	β^+ (100)	130.9 170.5	60® 100®	^{92}Mo$(\gamma,4\mathrm{n})$ ^{94}Mo$(\gamma,6\mathrm{n})$ ^{95}Mo$(\gamma,7\mathrm{n})$	−46.407 −64.154 −71.523	46.419 64.178 71.552

where n is the number of target atoms and $\langle\sigma\rangle$ is the average activation cross-section of the ^{197}Au$(\gamma,\mathrm{n})^{196}$Au and ^{27}Al$(\gamma,2\mathrm{pn})^{24}$Na reactions. $\Phi = \int_{E_{\mathrm{th}}}^{E_{\mathrm{e}}} \varphi$ is the bremsstrahlung flux with photon flux φ from the threshold value (E_{th}) to the bremsstrahlung end-point energy (E_{e}) [57]. a is the abundance or the branching ratio or the absolute γ-ray emission probability of the analyzed γ-rays and ε is the efficiency of the detector system for the γ-ray of the reaction product of interest. t, T, CL and LT are the irradiation time, cooling time, real time and live time, respectively. λ is the decay constant ($= \ln 2/T_{1/2}$) for the isotope of interest.

The γ-ray energies and the decay data for the residual nuclide such as branching ratio, half-lives used in eq. (1) for the nuclides of present interest are taken from refs. [21–24] and given in table 1. In the same table, the Q-values and threshold energies of the products from the $^{\mathrm{nat}}$Mo$(\gamma,x\mathrm{n})$ reactions are also shown. The average cross-section ($\langle\sigma\rangle$) for the ^{197}Au$(\gamma,\mathrm{n})^{196}$Au reaction used in eq. (1) for different bremsstrahlung end-point energies was calculated by using the following relation:

$$\langle\sigma\rangle = \frac{\sum \sigma\varphi}{\sum \varphi}. \qquad (2)$$

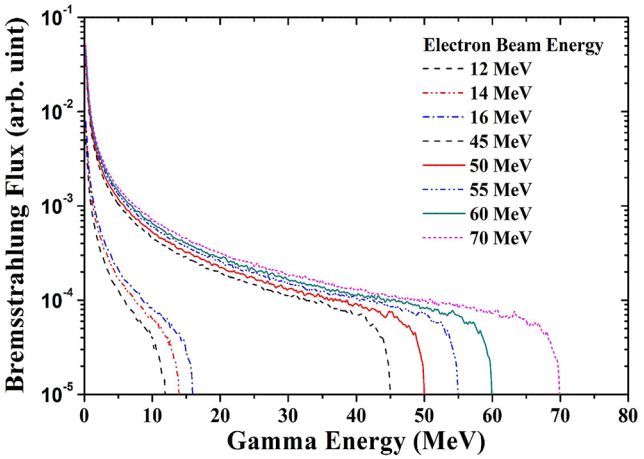

Fig. 3. Plot of bremsstrahlung spectrum for the end-point energies of 12, 14, 16, 45, 50, 55, 60, and 70 MeV calculated by using the GEANT4 code [60].

For the bremsstrahlung end-point energies of 12, 14 and 16 MeV, the photon flux (φ) distributions were calculated by using the GEANT4 code [60] and presented in fig. 3. The ^{197}Au$(\gamma,\mathrm{n})^{196}$Au reaction cross-section (σ)

Table 2. Flux conversion ratios (factor) used to obtain the photon flux for different reactions of ^{nat}Mo from the total flux based on the ^{197}Au$(\gamma,n)^{196}$Au and ^{27}Al$(\gamma,2pn)^{24}$Na reactions monitors.

Bremsstrahlung Energy (MeV)	12	14	16	45	50	55	60	70
$\langle\sigma\rangle$ of ^{197}Au$(\gamma,n)^{196}$Au (mb)	98.92	173.0	221.4	118.5	113.0	106.3	101.8	95.74
$\langle\sigma\rangle$ of ^{27}Al$(\gamma,2pn)^{24}$Na (mb)	–	–	–	0.045	0.068	0.092	0.116	0.158
^{100}Mo$(\gamma,n)/^{197}$Au(γ,n) *i.e.* $(8.3-E_\gamma)/(8.0-E_\gamma)$	0.919	0.941	0.953	0.982	0.984	0.983	0.972	1.050
^{100}Mo$(\gamma,n)/^{27}$Al$(\gamma,2pn)$ *i.e.* $(8.3-E_\gamma)/(31.4-E_\gamma)$	–	–	–	6.483	5.167	4.447	3.587	3.335
^{92}Mo$(\gamma,n)/^{197}$Au(γ,n) *i.e.* $(12.7-E_\gamma)/(8.0-E_\gamma)$	–	0.107	0.253	0.687	0.704	0.717	0.725	0.793
^{92}Mo$(\gamma,n)/^{27}$Al$(\gamma,2pn)$ *i.e.* $(12.7-E_\gamma)/(31.4-E_\gamma)$	–	–	–	4.427	3.596	3.121	2.821	2.463
^{94}Mo$(\gamma,3n)/^{27}$Al$(\gamma,2pn)$ *i.e.* $(30.4-E_\gamma)/(31.4-E_\gamma)$	–	–	–	1.107	1.081	1.067	1.058	1.046
^{95}Mo$(\gamma,4n)/^{27}$Al$(\gamma,2pn)$ *i.e.* $(37.8-E_\gamma)/(31.4-E_\gamma)$	–	–	–	0.414	0.547	0.627	0.677	0.447
^{92}Mo$(\gamma,2n)/^{27}$Al$(\gamma,2pn)$ *i.e.* $(22.8-E_\gamma)/(31.4-E_\gamma)$	–	–	–	2.146	1.871	1.715	1.616	1.498
^{94}Mo$(\gamma,4n)/^{27}$Al$(\gamma,2pn)$ *i.e.* $(40.5-E_\gamma)/(31.4-E_\gamma)$	–	–	–	0.225	0.394	0.498	0.565	0.647
^{95}Mo$(\gamma,5n)/^{27}$Al$(\gamma,2pn)$ *i.e.* $(47.9-E_\gamma)/(31.4-E_\gamma)$	–	–	–	–	0.046	0.183	0.287	0.420
^{92}Mo$(\gamma,3n)/^{27}$Al$(\gamma,2pn)$ *i.e.* $(36.0-E_\gamma)/(31.4-E_\gamma)$	–	–	–	0.561	0.662	0.723	0.761	0.805
^{94}Mo$(\gamma,5n)/^{27}$Al(γ,n) *i.e.* $(53.8-E_\gamma)/(31.4-E_\gamma)$	–	–	–	–	–	0.016	0.119	0.276
^{92}Mo$(\gamma,4n)/^{27}$Al$(\gamma,2pn)$ *i.e.* $(46.4-E_\gamma)/(31.4-E_\gamma)$	–	–	–	–	0.103	0.242	0.341	0.465
^{94}Mo$(\gamma,6n)/^{27}$Al(γ,n) *i.e.* $(64.2-E_\gamma)/(31.4-E_\gamma)$	–	–	–	–	–	–	–	0.070

for the mono-energetic photons has been determined by several authors [61–65]. In order to examine the literature data, we have calculated the ^{197}Au$(\gamma,n)^{196}$Au reaction cross-section by using the computer code TALYS 1.6 [54] and plotted in fig. 4. A short description of the computer code TALYS 1.6 is given in the next section. The literature data from ref. [65] is also shown in fig. 4 and is found to be in good agreement with the calculated values from TALYS 1.6 [54]. Thus it is acceptable to use the extrapolation and interpolation of the experimental data based on calculated values of TALYS. For the bremsstrahlung end-point energies of the present work, the ^{197}Au$(\gamma,n)^{196}$Au reaction cross-section from TALYS (fig. 4) was folded with the photon flux (fig. 3) to calculate the flux-weighted average ^{197}Au$(\gamma,n)^{196}$Au reaction cross-section ($\langle\sigma\rangle$), which is shown in table 2. Then, the experimental bremsstrahlung flux (Φ) for the ^{197}Au$(\gamma,n)^{196}$Au reaction was calculated by using the flux-weighted cross-section value ($\langle\sigma\rangle$) in eq. (1) with the rearrangement of terms. The threshold (E_{th}) for the ^{197}Au$(\gamma,n)^{196}$Au, ^{100}Mo$(\gamma,n)^{99}$Mo and ^{92}Mo$(\gamma,n)^{91}$Mo reactions are 8.073, 8.292 and 12.671 MeV, respectively. Thus the photon flux obtained from the ^{197}Au$(\gamma,n)^{196}$Au reaction has to be modified for the ^{100}Mo$(\gamma,n)^{99}$Mo and ^{92}Mo$(\gamma,n)^{91}$Mo reactions. This is based on their threshold value (E_{th}) to the bremsstrahlung end-point energy (E_e). In the case of ^{100}Mo$(\gamma,n)^{99}$Mo reaction at the bremsstrahlung end-point energies (E_e) of 12, 14 and 16 MeV, the weighted average flux obtained from the ^{197}Au$(\gamma,n)^{196}$Au reaction was multiplied by the factors of 0.919, 0.941 and

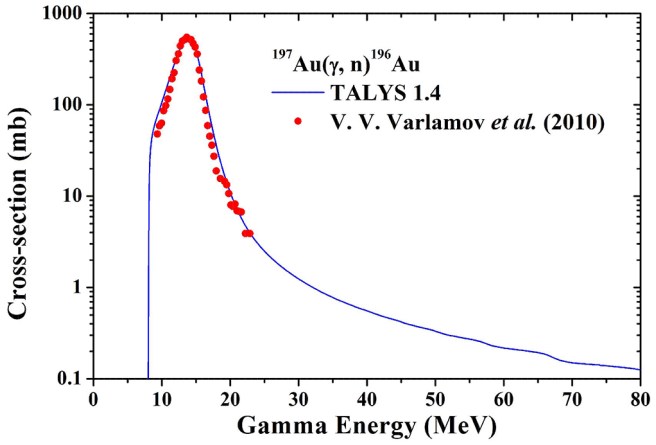

Fig. 4. Cross-sections of ^{197}Au$(\gamma, \mathrm{n})^{196}$Au reaction as a function of gamma energy obtained from the experimental data [65] and the calculated values from the TALYS [54] based on the mono-energetic photons.

0.953, respectively. These factors are the flux ratios for the ^{100}Mo$(\gamma, \mathrm{n})^{99}$Mo reaction from 8.292 MeV to 12, 14 and 16 MeV divided by the ^{197}Au$(\gamma, \mathrm{n})^{196}$Au reaction from 8.073 MeV to 12, 14 and 16 MeV, respectively. As an example the calculation of flux conversion ratio (factor) at the bremsstrahlung end-point energy of E_e for ^{100}Mo$(\gamma, \mathrm{n})^{99}$Mo reaction, the following formula was used:

$$\text{Factor} = \int_{E_{\mathrm{th}-\mathrm{Mo}}}^{E_\mathrm{e}} \varphi \, \mathrm{d}\varphi \Big/ \int_{E_{\mathrm{th}-\mathrm{Au}}}^{E_\mathrm{e}} \varphi \, \mathrm{d}\varphi. \qquad (3)$$

For this purpose the photon flux (φ) distribution was simulated by the GEANT4 code [60] and used for the renormalization of the experimental flux based on the monitor ^{197}Au$(\gamma, \mathrm{n})^{196}$Au reaction. In the case of $^{\mathrm{nat}}$Mo$(\gamma, \mathrm{n})^{91}$Mo reaction at the bremsstrahlung end-point energies of 14 and 16 MeV, 100% reaction cross-sections come from the ^{92}Mo$(\gamma, \mathrm{n})^{91}$Mo reaction due to the threshold value of 12.671 MeV. Thus for the ^{92}Mo$(\gamma, \mathrm{n})^{91}$Mo reaction at the bremsstrahlung end-point energies (E_e) of 14 and 16 MeV, the weighted average flux obtained from the ^{197}Au$(\gamma, \mathrm{n})^{196}$Au reaction was multiplied by the factors of 0.107 and 0.253, respectively. The different flux conversion ratio (factor) for the ^{100}Mo$(\gamma, \mathrm{n})^{99}$Mo and ^{92}Mo$(\gamma, \mathrm{n})^{91}$Mo reactions to the total flux of the ^{197}Au$(\gamma, \mathrm{n})^{196}$Au reaction are based on their different threshold values. For the ^{100}Mo$(\gamma, \mathrm{n})^{99}$Mo and ^{92}Mo$(\gamma, \mathrm{n})^{91}$Mo reactions at the bremsstrahlung end-point energies of 12, 14 and 16 MeV, the flux conversion ratios (factors) are given in table 2.

For the bremsstrahlung irradiations of 45–70 MeV, the photon flux (φ) distribution were also calculated by using the GEANT4 code [60] and presented in fig. 3. The experimental bremsstrahlung flux (Φ) during an individual irradiation was obtained from the observed activities (A_net) of the 332.98, 355.7 and 426.0 keV γ-lines of ^{196}Au from the ^{197}Au(γ, n) reaction as well as the 1368.6 keV γ-line of ^{24}Na from the ^{27}Al$(\gamma, 2\mathrm{pn})$ reaction. For the ^{197}Au$(\gamma, \mathrm{n})^{196}$Au reaction, the average cross-section ($\langle\sigma\rangle$) for the ^{197}Au$(\gamma, \mathrm{n})^{196}$Au reaction was calculated from the σ value of TALYS [54] for mono-energetic photons by using eq. (2). This is because for the ^{197}Au$(\gamma, \mathrm{n})^{196}$Au reaction, the flux-weighted reaction cross-section ($\langle\sigma_\mathrm{R}\rangle$) from ref. [65] can be obtained only up to the bremsstrahlung end-point energy of 24 MeV. On the other hand, for the ^{27}Al$(\gamma, 2\mathrm{pn})^{24}$Na reaction, the $\langle\sigma_\mathrm{R}\rangle$ value within the bremsstrahlung end-point energy range of 45–70 MeV was found to be 0.045–0.2 mb [66], which was used in eq. (1) to obtain the experimental bremsstrahlung flux (Φ). The threshold value for the ^{27}Al$(\gamma, 2\mathrm{pn})^{24}$Na reaction is 31.447 MeV. $^{\mathrm{nat}}$Mo has many isotopes with isotopic composition of ^{92}Mo (14.84%), ^{94}Mo (9.25%), ^{95}Mo (15.92%), ^{96}Mo (16.68%), ^{97}Mo (9.55%), ^{98}Mo (24.13%) and ^{100}Mo (9.63%), respectively. Thus, the threshold values for the same product from the reactions of different Mo isotopes are different. As an example, the threshold values for the production cross-section of ^{91}Mo from the ^{92}Mo$(\gamma, \mathrm{n})^{91}$Mo, ^{94}Mo$(\gamma, 3\mathrm{n})^{91}$Mo, ^{95}Mo$(\gamma, 4\mathrm{n})^{91}$Mo and ^{96}Mo$(\gamma, 5\mathrm{n})^{91}$Mo reactions are 12.671, 30.423, 37.795, 46.954 MeV, respectively. Similarly, the reactions thresholds for different products from the same Mo isotope are different. As an example, the threshold values for the ^{92}Mo$(\gamma, 2\mathrm{n})^{91}$Mo, ^{92}Mo$(\gamma, 3\mathrm{n})^{89}$Mo, and ^{92}Mo$(\gamma, 4\mathrm{n})^{88}$Mo reactions are 22.781, 36.014, and 46.419 MeV, respectively. More than 93% formation cross-sections of ^{91}Mo, ^{90}Mo, ^{89}Mo and ^{88}Mo come from the (γ, n), $(\gamma, 2\mathrm{n})$, $(\gamma, 3\mathrm{n})$ and $(\gamma, 4\mathrm{n})$ reactions of ^{92}Mo (14.84%) in the $^{\mathrm{nat}}$Mo, which is described in the next section. Thus the photon flux obtained from the ^{197}Au$(\gamma, \mathrm{n})^{196}$Au and ^{27}Al$(\gamma, 2\mathrm{pn})^{24}$Na reactions have to be modified for the (γ, n), $(\gamma, 2\mathrm{n})$, $(\gamma, 3\mathrm{n})$ and $(\gamma, 4\mathrm{n})$ reactions of ^{92}Mo based on their threshold values to the bremsstrahlung end-point energy as described in eq. (3). As an example, the flux conversion ratio for the ^{92}Mo$(\gamma, \mathrm{n})^{91}$Mo reaction to the ^{197}Au$(\gamma, \mathrm{n})^{196}$Au reaction at the bremsstrahlung end-point energies of 14, 16, 45, 50, 55, 60 and 70 MeV are 0.107, 0.253, 0.687, 0.704, 0.717, 0.725 and 0.793, respectively. Similarly, the flux conversion ratio for the same ^{92}Mo$(\gamma, \mathrm{n})^{91}$Mo reaction to the ^{27}Al$(\gamma, 2\mathrm{pn})^{24}$Na reaction at the bremsstrahlung end-point energies of 45, 50, 55, 60 and 70 MeV are 4.427, 3.596, 3.121, 2.821 and 2.463, respectively. For the ^{92}Mo$(\gamma, \mathrm{n})^{91}$Mo reaction cross-section calculation, the flux conversion ratio based on the ^{197}Au$(\gamma, \mathrm{n})^{196}$Au reaction monitor was used. For the $(\gamma, 2\mathrm{n})$, $(\gamma, 3\mathrm{n})$ and $(\gamma, 4\mathrm{n})$ reactions of ^{92}Mo at the bremsstrahlung end-point energies of 45, 50, 55, 60 and 70 MeV, the weighted average flux obtained from the ^{27}Al$(\gamma, 2\mathrm{pn})^{24}$Na reaction monitor was multiplied by different flux conversion ratios (factors), which are shown in table 2.

3.2 Calculation of $^{\mathrm{nat}}$Mo$(\gamma, x\mathrm{n})$ reaction cross-sections and their yield percentage

The radio-nuclides observed from the $^{\mathrm{nat}}$Mo$(\gamma, x\mathrm{n})$ reactions are ^{99}Mo, ^{91}Mo$^{\mathrm{m,g}}$, ^{90}Mo, ^{89}Mo and ^{88}Mo having different half-lives and γ-ray energies. The net photo-peak activities (A_net) corresponding to the photo-peak of γ-lines for different reaction products were obtained from the

Table 3. The percentage of formation cross-section (Yields) of the different reaction products from the $^{nat}Mo(\gamma, xn)$ reactions calculated using the TALYS [54].

Reactions	12	14	16	45	50	55	60	70
$^{100}Mo(\gamma, n)^{99}Mo$	100	100	100	100	100	100	100	100
$^{92}Mo(\gamma, n)^{91}Mo$	100	100	100	99.100	98.550	98.020	97.540	96.790
$^{94}Mo(\gamma, 3n)^{91}Mo$	–	–	–	0.830	1.130	1.340	1.470	1.650
$^{95}Mo(\gamma, 4n)^{91}Mo$	–	–	–	0.070	0.310	0.620	0.880	1.150
$^{96}Mo(\gamma, 5n)^{91}Mo$	–	–	–	–	–	0.020	0.110	0.380
$^{97}Mo(\gamma, 6n)^{91}Mo$	–	–	–	–	–	–	0.01	0.03
$^{92}Mo(\gamma, 2n)^{90}Mo$	–	–	–	99.926	99.160	97.760	96.040	92.660
$^{94}Mo(\gamma, 4n)^{90}Mo$	–	–	–	0.074	0.840	2.160	3.380	4.790
$^{95}Mo(\gamma, 5n)^{90}Mo$	–	–	–	–	–	0.080	0.580	2.380
$^{96}Mo(\gamma, 6n)^{90}Mo$	–	–	–	–	–	–	–	–
$^{92}Mo(\gamma, 3n)^{89}Mo$	–	–	–	100	100	100	99.940	98.210
$^{94}Mo(\gamma, 5n)^{89}Mo$	–	–	–	–	–	–	0.610	1.730
$^{95}Mo(\gamma, 6n)^{89}Mo$	–	–	–	–	–	–	–	0.060
$^{96}Mo(\gamma, 7n)^{89}Mo$	–	–	–	–	–	–	–	–
$^{92}Mo(\gamma, 4n)^{88}Mo$	–	–	–	100	100	100	100	100
$^{94}Mo(\gamma, 6n)^{88}Mo$	–	–	–	–	–	–	–	–
$^{95}Mo(\gamma, 7n)^{88}Mo$	–	–	–	–	–	–	–	–

total photo-peak areas after subtracting the linear Compton background. From the net photo-peak area (A_{net}) of the γ-lines of ^{99}Mo, $^{91}Mo^{m,g}$ and ^{90}Mo, their formation cross-sections ($\langle\sigma\rangle$) in the $^{nat}Mo(\gamma, xn)$ reactions were calculated by using the following equation [57]:

$$\langle\sigma\rangle = \frac{A_{net}\left(\frac{CL}{LT}\right)\lambda}{N\Phi a\varepsilon(1-e^{-\lambda t})(e^{-\lambda T})(1-e^{-\lambda CL})}\,. \qquad (4)$$

All the terms in eq. (4) have the same meaning as in eq. (1). The nuclear spectroscopic data for the reaction products from the $^{nat}Mo(\gamma, xn)$ reactions used in eq. (4) were taken from refs. [21–24] and shown in table 1. It can be seen from table 1 that in the case of $^{nat}Mo(\gamma, xn)^{91}Mo$ reaction, meta-stable (m)- and ground (g)-state of $^{91m,g}Mo$ have suitable half-lives with high-intensity γ-rays. Thus, the $^{nat}Mo(\gamma, xn)^{91}Mo$ reaction cross-sections for m- and g-states and thus the total (m + g) cross-section were obtained at the bremsstrahlung end-point energies of 45–70 MeV. The reaction product ^{91g}Mo has a half-life of 15.49 min with 1581.04 keV γ-ray of very low (0.226%) intensity. In spite of that the $^{nat}Mo(\gamma, xn)^{91g}Mo$ reaction cross-section was possible to measure at the bremsstrahlung end-point energies of 45–70 MeV. The reaction product ^{90}Mo has a half-life of 5.56 h with γ-rays of very good intensity and thus the $^{nat}Mo(\gamma, xn)^{90}Mo$ reaction cross-section was possible to measure at the bremsstrahlung end-point energies of 45–70 MeV. The reaction products ^{89}Mo and ^{88}Mo have the short half-lives of 2.04 min and 8.0 min with very good intensities of the γ-rays. However, the $^{nat}Mo(\gamma, xn)^{89,88}Mo$ reaction cross-sections are very low and thus not possible to measure within the bremstrahlung end-point energies of the present work. In the case of $^{nat}Mo(\gamma, n)^{99}Mo$ reaction, ^{99}Mo has the half-life of 65.94 h with very good intensities of the γ-rays. Besides this, ^{99}Mo is produced only from the $^{100}Mo(\gamma, n)^{99}Mo$ reaction without any contributions from the other isotopes. In the cases of $^{nat}Mo(\gamma, xn)^{91,90,89,88}Mo$ reactions, there are some contributions from different Mo isotopes. The percentage of contribution for different reactions channels *i.e.* the yield (Y_i) can be calculated using the relation [67]

$$Y_i = \int_{E_{th}}^{E_{max}} C_i\sigma_i(E)\varphi(E)\,\mathrm{d}E \Big/ \sum \int_{E_{th}}^{E_{max}} C_i\sigma_i(E)\varphi(E)\,\mathrm{d}E, \qquad (5)$$

where C_i is the natural composition of the isotope in the i-th nuclear reaction, σ_i is the reaction cross-section and $\varphi(E)$ is the photon flux at energy E.

The theoretical reaction cross-section (σ_i) for different reaction channels from ^{nat}Mo was calculated using TALYS 1.6 [54] code, which is described in the next section. Then the normalized yield contribution to a particular product from reactions of different isotopes is shown in table 3. It can be seen from table 3 that more than 92% formation cross-sections of ^{91}Mo, ^{90}Mo, ^{89}Mo and ^{88}Mo comes from the (γ, n), $(\gamma, 2n)$, $(\gamma, 3n)$ and $(\gamma, 4n)$ reaction of ^{92}Mo (14.84%) in the ^{nat}Mo. Thus the cross-sections for the $^{nat}Mo(\gamma, n)^{99}Mo$ reaction at the bremsstrahlung end-point energies of 10–16 and 45–70 MeV as well as for the $^{nat}Mo(\gamma, xn)^{91}Mo$ reaction at 45–70 MeV were calculated based on the weighted average flux of the $^{197}Au(\gamma, n)^{196}Au$ reaction [54,65]. On the other hand, the cross-section for the $^{nat}Mo(\gamma, xn)^{90}Mo$ reaction at

Table 4. Relative $^{nat}Mo(\gamma, xn)^{99}Mo$, $^{nat}Mo(\gamma, xn)^{91m,g}Mo$ and $^{nat}Mo(\gamma, xn)^{90}Mo$ reactions cross-sections at the bremsstrahlung end-point energies of 10–16 and 45–70 MeV from the present work, literature data [52,53] and the flux-weighted values of TALYS [54].

Reactions	Bremsstrahlung Energy (MeV)	[Ref.]	Average reaction cross-section ($\langle\sigma\rangle = \sum Y_i\sigma_i$) (mb)			
			Experimental			TALYS [53]
			metastable-state	ground-state	Total	Total
$^{nat}Mo(\gamma, n)^{99}Mo$	10	[52]	–	–	0.994 ± 0.110	3.139
	12	This work	–	–	3.155 ± 0.189	4.025
	12.5	[52]	–	–	5.256 ± 0.379	4.285
	14	This work	–	–	4.971 ± 0.455	5.460
	16	This work	–	–	6.427 ± 0.630	6.722
	45	This work	–	–	3.226 ± 0.560	3.534
	50	This work	–	–	3.087 ± 0.389	3.361
	55	This work	–	–	3.262 ± 0.523	3.168
	60	This work	–	–	3.326 ± 0.423	3.033
	70	This work	–	–	2.530 ± 0.524	2.850
$^{nat}Mo(\gamma, xn)^{91}Mo$	14.5	–	–	–	–	1.745
	15	–	–	–	–	2.414
	16	–	–	–	–	3.760
	17	–	–	–	–	5.350
	18	–	–	–	–	6.560
	19	–	–	–	–	6.976
	21	–	–	–	–	7.033
	23	–	–	–	–	6.627
	25	–	–	–	–	6.221
	26.8	–	–	–	–	5.604
	29.5	–	–	–	–	5.000
	30	–	–	–	–	4.908
	45	[53]	2.360 ± 0.235	2.586 ± 0.260	4.946 ± 0.350	3.561
	50	[53]	2.118 ± 0.211	2.665 ± 0.334	4.783 ± 0.395	3.330
	55	[53]	1.845 ± 0.172	2.538 ± 0.295	4.382 ± 0.342	3.148
	60	[53]	1.658 ± 0.226	2.517 ± 0.256	4.174 ± 0.342	2.985
	70	[53]	1.372 ± 0.158	2.182 ± 0.251	3.554 ± 0.297	2.728
$^{nat}Mo(\gamma, xn)^{90}Mo$	45	This work	–	–	0.376 ± 0.024	0.347
	50	This work	–	–	0.382 ± 0.046	0.318
	55	This work	–	–	0.373 ± 0.038	0.301
	60	This work	–	–	0.371 ± 0.031	0.288
	70	This work	–	–	0.319 ± 0.026	0.272

the bremsstrahlung end-point energies of 45–70 MeV were calculated based on the weighted average flux of the $^{27}Al(\gamma, 2pn)^{24}Na$ reaction [66]. This is because for the (γ, n) reaction cross-sections calculation, it is better to use the $^{197}Au(\gamma, n)^{196}Au$ reaction monitor and for the $(\gamma, 2n)$ and higher reaction cross-sections calculation, it is better to use the $^{27}Al(\gamma, 2pn)^{24}Na$ reaction monitor. The use of monitors is purely based on their comparable threshold values of the monitor with those of the reactions of interest.

4 Results and discussion

In the present work, we determine the relative cross-section of the $^{nat}Mo(\gamma, n)^{99}Mo$ reaction at the

Table 5. Absolute ^{100}Mo$(\gamma,\mathrm{n})^{99}$Mo, ^{92}Mo$(\gamma,\mathrm{n})^{91\mathrm{m,g}}$Mo and ^{92}Mo$(\gamma,2\mathrm{n})^{90}$Mo reactions cross-sections at the bremsstrahlung end-point energies of 10–16 and 45–70 MeV from the present work, literature data [52,53] and the flux-weighted values of TALYS [54].

Reactions	Bremsstrahlung Energy (MeV)	[Ref.]	Average reaction cross-section ($\langle\sigma\rangle = \sum Y_i\sigma_i$) (mb)			
			Experimental			TALYS [53]
			metastable-state	ground-state	Total	Total
^{100}Mo$(\gamma,\mathrm{n})^{99}$Mo	10	[52]	–	–	10.320 ± 1.140	32.6
	12	This work	–	–	32.762 ± 1.960	41.8
	12.5	[52]	–	–	54.580 ± 3.940	44.5
	14	This work	–	–	51.623 ± 4.730	56.7
	16	This work	–	–	66.741 ± 6.540	69.8
	45	This work	–	–	33.501 ± 5.810	36.7
	50	This work	–	–	32.055 ± 4.040	34.9
	55	This work	–	–	33.872 ± 5.431	32.9
	60	This work	–	–	34.534 ± 4.390	31.5
	70	This work	–	–	26.274 ± 5.440	29.6
^{92}Mo$(\gamma,\mathrm{n})^{91}$Mo	14.5	–	–	–	–	11.759
	15	–	–	–	–	16.267
	16	–	–	–	–	25.337
	17	–	–	–	–	36.051
	18	–	–	–	–	37.466
	19	–	–	–	–	47.008
	21	–	–	–	–	47.392
	23	–	–	–	–	44.656
	25	–	–	–	–	41.921
	26.8	–	–	–	–	37.763
	29.5	–	–	–	–	33.693
	30	–	–	–	–	33.073
	45	[53]	15.903 ± 1.584	17.426 ± 1.752	33.329 ± 2.362	23.996
	50	[53]	14.272 ± 1.422	17.958 ± 2.251	32.230 ± 2.662	22.439
	55	[53]	12.433 ± 1.162	17.102 ± 1.988	29.535 ± 2.303	21.213
	60	[53]	11.173 ± 1.523	16.961 ± 1.725	28.134 ± 2.301	20.115
	70	[53]	9.245 ± 1.065	14.702 ± 1.694	23.947 ± 2.001	18.383
^{92}Mo$(\gamma,2\mathrm{n})^{90}$Mo	45	This work	–	–	2.715 ± 0.387	2.338
	50	This work	–	–	2.572 ± 0.354	2.143
	55	This work	–	–	2.752 ± 0.454	2.028
	60	This work	–	–	2.725 ± 0.180	1.941
	70	This work	–	–	2.230 ± 0.175	1.833

bremsstrahlung end-point energies of 12, 14, 16, 45, 50, 55, 60 and 70 MeV, which are given in table 4 along with the literature data at 10 and 12.5 MeV [52]. Similarly, the relative cross-sections of the $^{\mathrm{nat}}$Mo$(\gamma,x\mathrm{n})^{,90}$Mo reaction from the present work and for the $^{\mathrm{nat}}$Mo$(\gamma,x\mathrm{n})^{91}$Mo reaction from earlier work [53] at the bremsstrahlung end-point energies of 45, 50, 55, 60 and 70 MeV are given in table 4. During the calculation, isotopic composition of $^{\mathrm{nat}}$Mo sample used was based on the refs. [22,23]. Thus the $^{\mathrm{nat}}$Mo$(\gamma,\mathrm{n})^{99,91,90}$Mo reaction cross-sections shown in table 4 are relative one. This has been updated after using isotopic composition from refs. [22,23]. The absolute ^{100}Mo$(\gamma,\mathrm{n})^{99}$Mo, ^{92}Mo$(\gamma,\mathrm{n})^{91}$Mo and ^{92}Mo$(\gamma,2\mathrm{n})^{90}$Mo reaction cross-sections were shown in table 5.

The uncertainties associated in the measured reaction cross-sections come from the replicate measurements. The overall uncertainty is the quadratic sum of both random and systematic errors, which was done based on the refs. [68,69]. The $^{\mathrm{nat}}$Mo$(\gamma,x\mathrm{n})^{99}$Mo reaction at the bremsstrahlung end-point energies of 12, 14 and 16 MeV

are based on the 20 MeV electron linac (ELBE) at HZDR, Germany. The random errors are due to uncertainties in i) sample mass (0.5%), ii) counting statistics (7–10%) and iii) reproducibility of counting geometry (0.5%). The systematic errors are due to uncertainties in i) the simulated bremsstrahlung spectrum due to the use of GEANT4 code (2%); ii) the experimental photon flux due to the use of ^{197}Au$(\gamma, \mathrm{n})^{196}$Au reaction monitor reaction cross-section ($\sim$ 3%); iii) irradiation time (0.25%); iv) detection efficiency calibration due to the use of different standard sources ($\sim$ 4%); v) the half-life of the reaction products and the γ-ray abundances ($\sim$ 2%). Thus the total random and systematic errors are about 7.04–10.01% and 5.75%, respectively. Then the overall uncertainty is found to be 9.09–11.54%.

The $^{\mathrm{nat}}$Mo$(\gamma, x\mathrm{n})^{99}$Mo, $^{\mathrm{nat}}$Mo$(\gamma, x\mathrm{n})^{91}$Mo and $^{\mathrm{nat}}$Mo$(\gamma, x\mathrm{n})^{90}$Mo reaction cross-sections at the bremsstrahlung end-point energies of 45, 50, 55, 60 and 70 MeV are based on the 100 MeV electron linac at PAL, Pohang, Korea. The random errors are due to uncertainties in i) sample mass (0.5%), ii) counting statistics (5–7%) and iii) reproducibility of counting geometry (0.5%). The systematic errors are due to uncertainties in i) the simulated bremsstrahlung spectrum due to the use of GEANT4 code (2%); ii) the experimental photon flux due to the use of ^{197}Au$(\gamma, \mathrm{n})^{196}$Au and ^{27}Al$(\gamma, 2\mathrm{pn})^{24}$Na reaction monitors reaction cross-sections ($\sim$ 5%); iii) irradiation time (0.5%); iv) detection efficiency calibration due to the use of standard ^{152}Eu source ($\sim$ 3%); v) the half-life of the reaction products and the γ-ray abundances ($\sim$ 2%). Thus the total random and systematic errors are about 5.05–7.04% and 6.5%, respectively. Then the overall uncertainty is found to be 8.23–9.58%.

The $^{\mathrm{nat}}$Mo$(\gamma, x\mathrm{n})^{90}$Mo reaction cross-section at the bremsstrahlung end-point energies of 45, 50, 55, 60 and 70 MeV are determined for the first time. The $^{\mathrm{nat}}$Mo$(\gamma, \mathrm{n})^{99}$Mo reaction cross-section at the bremsstrahlung end-point energies of 12, 14, 16, 45, 50, 55, 60 and 70 MeV are also determined for the first time. There are two values of the $^{\mathrm{nat}}$Mo$(\gamma, \mathrm{n})^{99}$Mo reaction cross-section available in our earlier work [52] at the bremsstrahlung end-point energies of 10 and 12.5 MeV based on the same activation and off-line γ-ray spectrometric technique. The ^{100}Mo$(\gamma, \mathrm{n})^{99}$Mo and ^{92}Mo$(\gamma, x\mathrm{n})^{91,90}$Mo reaction cross-sections for the mono-energetic photons from their threshold energies to 29.5 MeV are available in the literature [43–49]. For the ^{92}Mo$(\gamma, x\mathrm{n})^{89,88}$Mo reaction, the cross-sections are not available in the literature for any of the bremsstrahlung end-point energies or for the mono-energetic photons. Thus the relative $^{\mathrm{nat}}$Mo$(\gamma, x\mathrm{n})^{88\text{-}91,99}$Mo reaction cross-sections as a function of photon energy were calculated using TALYS code 1.6 [54].

The nuclear reaction cross-sections calculation in TALYS involve the projectiles like neutrons, photons, protons, deuterons, tritons, ^{3}He- and alpha-particles, in the energy range of 1 keV to 200 MeV and for target nuclides of mass 12 and heavier. In TALYS calculation several options are included for the choice of different parameters such as γ-ray strength functions, nuclear level densities and nuclear model parameters, etc. The level density parameters in TALYS 1.6 are calculated using six different choices of the level density model. The TALYS1.6 program provides two options for spin distribution for the residual states after pre-equilibrium emission. The default option is to adopt the compound nucleus spin distribution. Another option is to assign a spin distribution to the particle-hole state density. Pre-equilibrium processes cover a sizable part of the reaction cross-section for the incident energies between 10 to 200 MeV. The reaction cross-sections measured in the present work are above the bremsstrahlung end-point energy of 10 MeV. So it is better to assign a spin distribution to the particle-hole state. Global adjustable constant for the spin cut-off parameter for all nuclides in the calculations ranges from 0 to 10. We have done the calculation of $^{\mathrm{nat}}$Mo$(\gamma, x\mathrm{n})$ reaction cross-section by using the default parameters with the choice of the level density models, γ-ray strength functions and adjustable constant for spin cut-off parameter. All possible outgoing channels *i.e.* (γ, x) reactions for a given photon energy with different Mo isotopes were considered. Among these only the $(\gamma, x\mathrm{n})$ reaction cross-sections for different isotopes of Mo were picked up. It can be seen from table 3 that for all the bremsstrahlung energies, the production of ^{99}Mo takes place only from the ^{100}Mo(γ, n) reaction. On the other hand, within the bremsstrahlung end-point energy of 70 MeV, the production of ^{91}Mo can takes place from the ^{92}Mo(γ, n), ^{94}Mo$(\gamma, 3\mathrm{n})$, ^{95}Mo$(\gamma, 4\mathrm{n})$, ^{96}Mo$(\gamma, 5\mathrm{n})$ and ^{97}Mo$(\gamma, 6\mathrm{n})$ reactions. Among these reactions, more than 96% contribution of ^{91}Mo comes from the ^{92}Mo(γ, n) reaction. Similarly, within the bremsstrahlung energy of 70 MeV, the production of ^{90}Mo can takes place from the ^{92}Mo$(\gamma, 2\mathrm{n})$, ^{94}Mo$(\gamma, 4\mathrm{n})$ and ^{95}Mo$(\gamma, 5\mathrm{n})$ reactions. Among these reactions, more than 92% contribution of ^{90}Mo comes only from the ^{92}Mo$(\gamma, 2\mathrm{n})$ reaction. Thus the contribution for the formation cross-sections of ^{91}Mo, ^{90}Mo, ^{89}Mo and ^{88}Mo are very less or negligible from the heavier-mass Mo isotopes.

The formation cross-section of ^{99}Mo, ^{91}Mo, ^{90}Mo, ^{89}Mo and ^{88}Mo from different Mo isotopes are plotted in figs. 5–9 as a function of photon energy. In the same figures, the isotopic average formation cross-sections of each reaction products from $^{\mathrm{nat}}$Mo are also plotted as a function of photon energy. The experimental ^{100}Mo$(\gamma, \mathrm{n})^{99}$Mo, ^{92}Mo$(\gamma, \mathrm{n})^{91}$Mo and ^{92}Mo$(\gamma, 2\mathrm{n})^{90}$Mo reaction cross-sections for mono-energetic photons from refs. [43–49] are also plotted in figs. 5–9 for comparison. The absolute ^{100}Mo$(\gamma, \mathrm{n})^{99}$Mo, ^{92}Mo$(\gamma, \mathrm{n})^{91}$Mo and ^{92}Mo$(\gamma, 2\mathrm{n})^{90}$Mo reaction cross-sections from refs. [43–49] were multiplied by its isotopic abundance to make them relative to compared with the $^{\mathrm{nat}}$Mo$(\gamma, x\mathrm{n})^{99,91,90}$Mo reaction cross-sections of TALYS. It can be seen from figs. 5–9 that, the theoretical ^{100}Mo$(\gamma, \mathrm{n})^{99}$Mo, ^{92}Mo$(\gamma, \mathrm{n})^{91}$Mo and ^{92}Mo$(\gamma, 2\mathrm{n})^{90}$Mo reaction cross-sections as a function of photon energy from TALYS 1.6 shows a similar structure of the available experimental data [43–49]. In literature, the experimental data for ^{92}Mo$(\gamma, 3\mathrm{n})^{89}$Mo and ^{92}Mo$(\gamma, 4\mathrm{n})^{88}$Mo reactions are not available to compare with the theoretical estimate of TALYS.

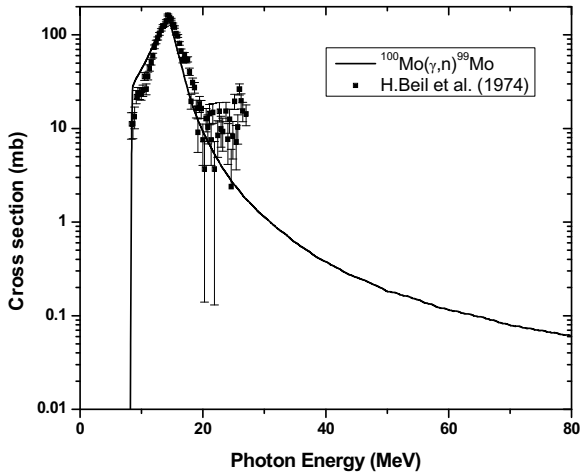

Fig. 5. Cross-sections of $^{100}\mathrm{Mo}(\gamma, x\mathrm{n})^{99}\mathrm{Mo}$ reaction as a function of gamma energy obtained from the experimental data [47] and the calculated values from the TALYS [54] based on the mono-energetic photons.

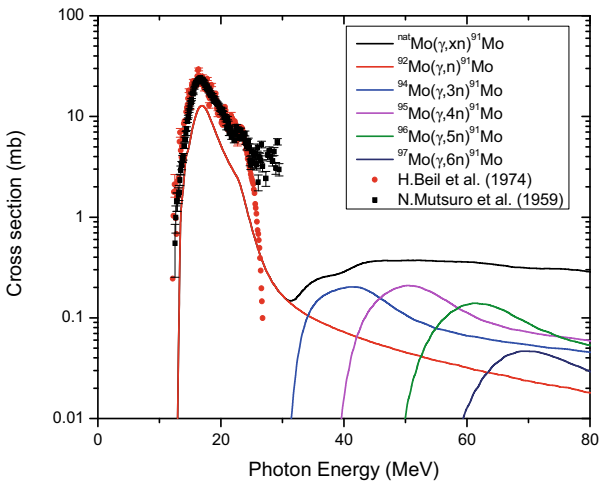

Fig. 6. Cross-sections of $^{\mathrm{nat}}\mathrm{Mo}(\gamma, x\mathrm{n})^{91}\mathrm{Mo}$ reaction as a function of gamma energy obtained from the experimental data [45, 47] and the calculated values from the TALYS [54] based on the mono-energetic photons.

The relative flux-weighted average $^{\mathrm{nat}}\mathrm{Mo}(\gamma, \mathrm{n})^{99}\mathrm{Mo}$ and $^{\mathrm{nat}}\mathrm{Mo}(\gamma, x\mathrm{n})^{91\text{-}88}\mathrm{Mo}$ reaction cross-sections were obtained from the theoretical values of TALYS 1.6 based on mono-energetic photon by using the eq. (2). The flux-weighted TALYS values at different bremsstrahlung end-point energies are given in table 4 for comparison. It can be seen from table 4 that the experimentally obtained flux-weighted average $^{\mathrm{nat}}\mathrm{Mo}(\gamma, \mathrm{n})^{99}\mathrm{Mo}$, $^{\mathrm{nat}}\mathrm{Mo}(\gamma, x\mathrm{n})^{91}\mathrm{Mo}$ and $^{\mathrm{nat}}\mathrm{Mo}(\gamma, x\mathrm{n})^{90}\mathrm{Mo}$ reaction cross-sections of the present work at the bremsstrahlung end-point energies of 10–16 and 45–70 MeV are in good agreement with the flux-weighted value of TALYS [54]. The relative flux-weighted average $^{100}\mathrm{Mo}(\gamma, \mathrm{n})^{99}\mathrm{Mo}$, $^{92}\mathrm{Mo}(\gamma, \mathrm{n})^{91}\mathrm{Mo}$ and $^{92}\mathrm{Mo}(\gamma, 2\mathrm{n})^{90}\mathrm{Mo}$ reaction cross-sections were also calculated from the literature data [43–49] based on the mono-energetic photons and plotted in fig. 10 along with

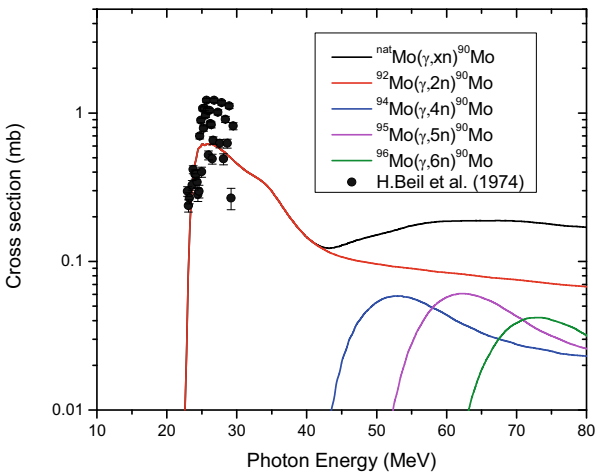

Fig. 7. Cross-sections of $^{\mathrm{nat}}\mathrm{Mo}(\gamma, x\mathrm{n})^{90}\mathrm{Mo}$ reaction as a function of gamma energy obtained from the experimental data [45, 47] and the calculated values from the TALYS [54] based on the mono-energetic photons.

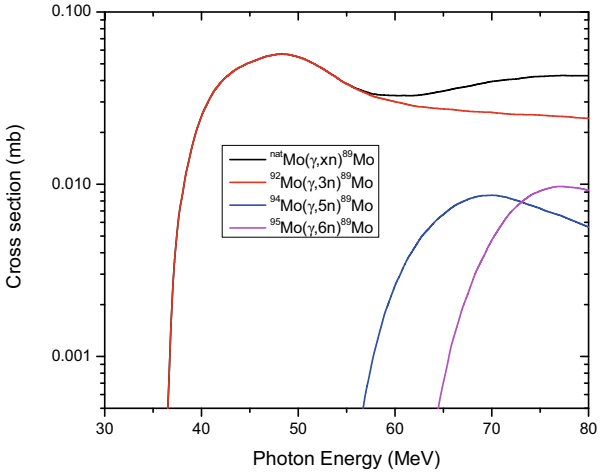

Fig. 8. Cross-sections of $^{\mathrm{nat}}\mathrm{Mo}(\gamma, x\mathrm{n})^{89}\mathrm{Mo}$ reaction as a function of gamma energy obtained from the calculated values of the TALYS [54] based on mono-energetic photons.

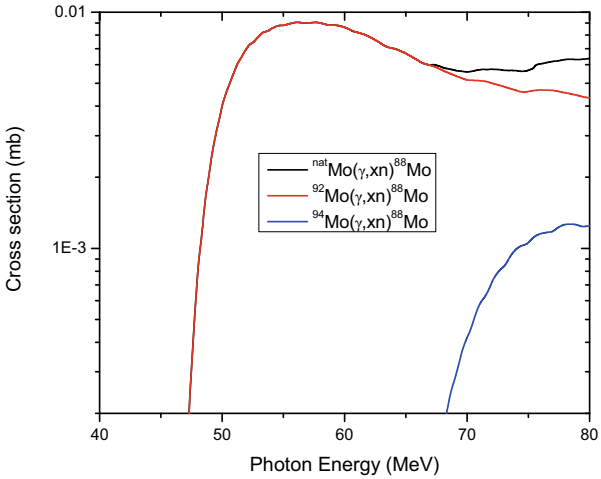

Fig. 9. Cross-sections of $^{\mathrm{nat}}\mathrm{Mo}(\gamma, x\mathrm{n})^{88}\mathrm{Mo}$ reaction as a function of gamma energy obtained from the calculated values of the TALYS [54] based on mono-energetic photons.

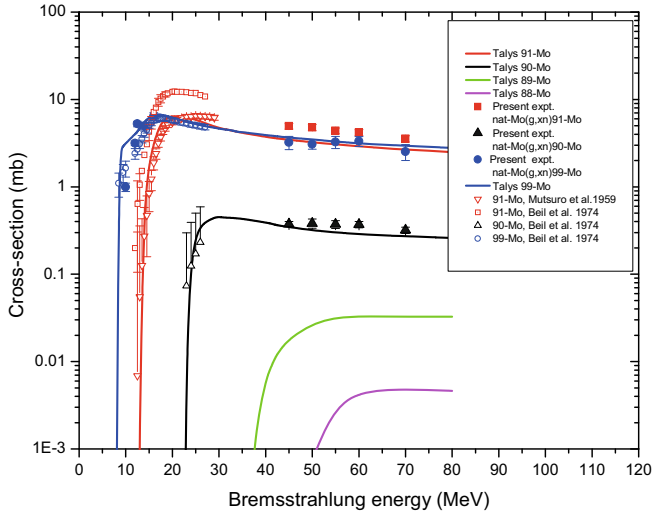

Fig. 10. Cross-sections of $^{nat}Mo(\gamma, xn)^{88\text{-}91,99}Mo$ reactions of the present and earlier work [52,53] as a function of bremsstrahlung end-point energy as well as the flux-weighted values from the literature data [45,47] and the calculated values of the TALYS [54].

the present data from table 4 and theoretical values from TALYS. It can be seen from fig. 10 that the experimentally obtained $^{nat}Mo(\gamma, n)^{99}Mo$ reaction cross-section from the present work and our earlier data [52] at the bremsstrahlung end-point energies of 10–16 and 45–70 MeV as well as the flux-weighted literature data [47] within 27 MeV are in close agreement with TALYS values. Similarly, the $^{nat}Mo(\gamma, xn)^{90}Mo$ reaction cross-section from the present work within 45–70 MeV and the flux-weighted values from Beil *et al.* data [47] within 29.5 MeV are also in agreement with the TALYS values within the uncertainty limits. In the case of $^{nat}Mo(\gamma, xn)^{91}Mo$ reaction, the flux-weighted average cross-section from Mutsuro data [45] within 27 MeV and our earlier data [53] within 45–70 MeV are also in good agreement with the values from TALYS. However, the flux-weighted values from Beil *et al.* data [47] within 29.5 MeV are significantly higher than the theoretical estimate of TALYS.

Further from fig. 10, it can be seen that the experimental and theoretical $^{nat}Mo(\gamma, xn)^{99}Mo$ and $^{nat}Mo(\gamma, xn)^{91}Mo$ reaction cross-sections increase very sharply from the threshold values to 15–17 MeV. Above 15–17 MeV, it increases slowly and remains constant up to 23 MeV due to the opening of $^{nat}Mo(\gamma, 2n)^{90}Mo$ reaction channel. There after the cross-section slowly decreases up to the bremsstrahlung end-point energy of 70 MeV due to the opening of other reactions channels. Similarly, the experimental and theoretical $^{nat}Mo(\gamma, xn)^{90}Mo$ reaction cross-section increases very sharply from the threshold value of 23 MeV to 27 MeV. Above 27 MeV, it increases very slowly up to 30 MeV and then remains constant up to 36 MeV, *i.e.* up to the opening of $^{nat}Mo(\gamma, xn)^{89}Mo$ reaction channel. There after the cross-section slowly decreases up to the bremsstrahlung end-point energy of 70 MeV due to the opening of other reactions channels. The theoretical and experimental cross-sections of $^{nat}Mo(\gamma, xn)^{89,88}Mo$ reactions also show similar trend (fig. 10) as of $^{nat}Mo(\gamma, xn)^{99}Mo$ and $^{nat}Mo(\gamma, xn)^{91,90}Mo$ reaction channels. The individual reaction, first increases sharply from its respective threshold value to a particular value and remains constant to a certain extent, where other reaction channels start increasing. Then it starts decreasing due to the contribution of excitation energy to the other reaction channels. The above observations indicate the role of excitation energy and its partition in to different reaction channels. Besides the above observations, it can be seen from fig. 10 that the increasing trend of cross-section from its threshold value up to the opening of the next channel are more pronounced for the $^{nat}Mo(\gamma, xn)^{99}Mo$ and $^{nat}Mo(\gamma, xn)^{91,90}Mo$ reactions compared to $^{nat}Mo(\gamma, xn)^{89,88}Mo$ reactions. This is because the increasing trend of $^{nat}Mo(\gamma, xn)^{99}Mo$ and $^{nat}Mo(\gamma, xn)^{91,90}Mo$ reaction cross-sections lies within 8–23 MeV, where GDR effect plays its role.

From the above discussion, it is clear that the production of ^{99}Mo activity from the $^{nat}Mo(\gamma, xn)$ and $^{100}Mo(\gamma, n)$ reactions within the bremsstrahlung end-point energy of GDR region has an advantage, which is important from the medical point of view. This is because there is a feasibility of the production of ^{99}Mo from the $^{100}Mo(\gamma, n)$ reaction as an alternative to the $^{100}Mo(n, 2n)$, $^{100}Mo(p, pn)$ and $^{98}Mo(n_{th}, \gamma)$ reactions. As obtained in the present work (table 5), the $^{100}Mo(\gamma, n)^{99}Mo$ reaction has a maximum cross-section of 66.741 mb at the bremsstrahlung end-point energy of 16 MeV. On the other hand, the production cross-section of ^{99}Mo is 152.3 mb for the $^{100}Mo(\gamma, n)$ reaction at the mono-energetic photon of 14.56 MeV [47], 162–180 mb for the $^{100}Mo(p, pn)$ reaction at E_p = 25–35 MeV [35,42] and 130 mb for the $^{98}Mo(n, \gamma)^{99}Mo$ reaction at E_n = 0.025 eV [50], respectively. In the proton energy of 25–35 MeV, other reaction products also produce along with ^{99}Mo. Besides this, generating sufficient high-energy proton flux is not easy to achieve. Similarly, producing mono-energetic photon with sufficient flux is also a difficult task. On the other hand production of bremsstrahlung energy from the electron linac with a reasonable cost is an easy task. Thus the production of ^{99}Mo activity from the $^{nat}Mo(\gamma, xn)$ and $^{100}Mo(\gamma, n)$ reactions at bremsstrahlung end-point energies within GDR region from electron linac is a relevant and novel approach, which provides alternative routes to $^{235}U(n, f)$ and $^{98}Mo(n, \gamma)$ reactions, circumventing the need for a reactor.

The activity of ^{99}Mo produced from the $^{nat}Mo(\gamma, n)$ and $^{100}Mo(\gamma, n)$ reactions at different bremsstrahlung end-point energies has been shown in our earlier work [51]. It has also been shown by us [51] that it is possible to fulfil the medical requirements of ^{99}Mo from the $^{nat}Mo(\gamma, xn)$ and $^{100}Mo(\gamma, n)$ reactions as per imaging demand all over the world [70]. It has many advantages compared to the existing method of commercial production from the $^{235}U(n, f)$ and $^{98}Mo(n, \gamma)$ reaction. This is because, it is possible to install electron linacs at a lower cost, very near to the medical centres, which reduces the transport time and does not need enhanced security and other safeguards unlike nuclear reactors. Besides this, it is possible to halt

and re-start the electron accelerator for isotope production through the $^{nat}Mo(\gamma, xn)$ and $^{100}Mo(\gamma, n)$ reactions according to demand, something that cannot be achieved with a nuclear reactor through $^{235}U(n, f)$ and $^{98}Mo(n, \gamma)$ reactions.

5 Conclusions

i) The $^{nat}Mo(\gamma, n)^{99}Mo$ and $^{nat}Mo(\gamma, xn)^{91,90}Mo$ reaction cross-sections at the bremsstrahlung end-point energies of 12–16 MeV and 45–70 MeV have been determined using activation and off-line γ-ray spectrometric technique.

ii) The $^{nat}Mo(\gamma, xn)^{88\text{-}91,99}Mo$ reaction cross-sections as a function of mono-energetic photon energy was theoretically calculated using the TALYS 1.6 code. The flux-weighted average reaction cross-sections at different bremsstrahlung end-point energies were then obtained from the theoretical values of TALYS and the literature data based on mono-energetic photon and are found to be in good agreement.

iii) The experimental and theoretical $^{nat}Mo(\gamma, xn)^{90,91,99}Mo$ reaction cross-sections increase from the threshold value to a certain value, where other reaction channel opens up. Then it remains constant up to certain energy, where other reaction starts increasing. Thereafter they decrease, when the next reaction channels remain constant. This indicates the effect of excitation energy and its partition in different reaction channels.

iv) Within the end-point bremsstrahlung of 17–23 MeV, the increasing trend of cross-sections for the $^{nat}Mo(\gamma, xn)^{90,91,99}Mo$ reactions is sharper than the $^{nat}Mo(\gamma, xn)^{89,88}Mo$ reactions. This indicates pronounced GDR effect besides the role of excitation energy within the bremsstrahlung end-point energy of 23 MeV.

v) For the production of ^{99}Mo, the $^{nat}Mo(\gamma, xn)$ and $^{100}Mo(\gamma, n)$ reactions provide an alternative route in comparison with the $^{98}Mo(n, \gamma)$ and $^{235}U(n, f)$ reactions circumventing the need for a reactor. Thus it is possible to produce the medical needs of ^{99}Mo from the $^{nat}Mo(\gamma, xn)$ and $^{100}Mo(\gamma, n)$ reactions to fulfil the requirement of the imaging procedure all over the world.

The authors are thankful to the staff of the electron linacs ELBE at HZDR, Dresden, Germany and PAL, Pohang, Korea for providing the electron beam to carry out the experiments. One of the author Dr. HN is thankful to the IAEA for giving the IAEA-CRP project No. 17443/R0 and BRAIN pool program under KOFEST, Korea, for inviting him as visiting professor to the department of high-energy physics, Daegu, as well as giving financial support to travel to Dresden, Germany, to carry out the experiment. This research was partly supported by the IAEA and National Research Foundation of Korea (NRF) through a grant provided by the Korean Ministry of Education, Science & Technology (NRF-2010-0021375, NRF-2010-0018498).

References

1. IAEA, *Handbook on photonuclear data for applications cross-sections and spectra*, IAEA TECDOC-1178 (IAEA, Vienna, 2000) available online at `http://www-nds.iaea.org/publications/tecdocs/`.
2. IAEA, *Nuclear technology review, annex VIII: The socio-economics of nuclear applications: a perspective* (IAEA, Vienna, 2004) pp. 85–94.
3. IAEA, *Categorization of radioactive sources* - Revision of IAEA-TECDOC-1191 and IAEA-TECDOC-1344 (IAEA, Vienna, 2003).
4. National Council of Radiation Protection and Measurements (NCRP), *Sources and magnitude of occupational and public exposures from nuclear medicine procedures*, NCRP report no. 124, March 1996.
5. S. Groth, *Lasting benefits: Nuclear application in health care*, IAEA Bulletin, 42/1/2000, Vienna (2000).
6. C.L. Larsson *Availability and Use of Medical Isotopes in Canada*, TM 2004-218, OMB no. 0704-0188 (Defense Research and Development Canada (DRDC), Ottawa, 2004).
7. C.B. Cameron, J. Clin. Pathol. **23**, 280 (1970).
8. C. Schiepers, *Diagnostic Nuclear Medicine* (Springer, Berlin, 2006).
9. H.F. Royston, J.L. Jeremy, T. Pal Buckeley, L.D. Daniel, T.E. James, A. Paulenova, J. Chem. Educ. **83**, 625 (2006).
10. G.J.R. Cook, Clin. Nucl. Med. **1**, 5 (2006).
11. G.J.R. Cook, Br. J. Radiol. **76**, S152 (2003).
12. B. Scholten, R.M. Lambrecht, C. Michel, V.R. Hernan, S.M. Qaim, Appl. Radiat. Isot. **51**, 69 (1999).
13. P. Froment, I. Tilquin, M. Cogneau, Th. Delbar, J. Vervier, G. Ryckewaert, Nucl. Instrum. Methods Phys. Res. **493**, 165 (2002).
14. A.V. Sabel'nikov, O.D. Maslov, L.G. Molokanova, M.V. Gustova, S.N. Dmitriev, Radiokhimiya **48**, 172 (2006) or Radiochemistry **48**, 191 (2006).
15. IAEA, *Alternative technologies for ^{99m}Tc generators*, IAEA-TECDOC-852 (IAEA, Vienna, 1995) `http://www-pub.iaea.org/MTCD/publications/PDF/te_852_prn.pdf`.
16. IAEA, *Charged particle cross-section data base for medical radioisotope production: diagnostic radioisotopes and monitor reactions*, IAEA-TECDOC-1211 (IAEA, Vienna, 2001) `http://www-nds.iaea.org` (accessed May 2001).
17. T. Ruth, Nature **457**, 536 (2009).
18. IAEA, *Nuclear technology review, annex VIII: Production and supply of molybdenum-99*, IAEA/NTR/2010 (IAEA, Vienna, 2010) pp. 150–167.
19. J.P. Gambini, P. Cabral, O. Alonso, E. Savio, S.D. Figueroa, X. Zhang, M. Lixin, L.D. Susan, P.Q. Thomas, Nucl. Med. Biol. **38**, 255 (2011).
20. M.A. Terán, M. Elena, A.L Reyes, P. Andrea, V. Marcelo, E. Patricia, P.P. Jose, S. Eduardo, Nucl. Med. Biol. **38**, 279 (2011).
21. NuDat 2.6, National Nuclear Data Center, Brookhaven National Laboratory, updated 2011, available on-line at `http://www.nndc.bnl.gov/`.
22. R.B. Firestone, L.P. Ekstrom, *Table of Radioactive Isotopes*, Lawrence Berkeley National Laboratory, Berkeley Version 2.1 (2004) `http://ie.lbl.gov/toi/index.asp`.
23. E. Browne, R.B. Firestone, in *Table of Radioactive Isotopes*, edited by V.S. Shirley (Wiley, New York, 1986).
24. J. Blachot, C. Fiche, Ann. Phys. Suppl. **6**, 3 (1981).

25. P. Richards, Brookhaven National Laboratory, Report no. BNL 9601 (BNL Long Island, 1965).
26. H. Arino, J.C. Frank, D.G. Kenneth, K.T. Alfred, US Patent3, 940, 318, 24 February 1976.
27. J. Bourges, C. Madic, G. Koehly, H. Nguyent, D. Baltes, C. Landesman, A. Simon, Nucl. Technol. **113**, 204 (1996).
28. M.M. Rahman, S.M. Qaim, Nucl. Phys. A **435**, 43 (1985).
29. P. Reimer, V. Avrigeanu, S.V. Chuvaev, A.A. Filatenkov, T. Glodariu, A. Koning, A.J.M. Plompen, S.M. Qaim, D.L. Smith, H. Weigmann, Phys. Rev. C **71**, 044617 (2005).
30. V. Semkova, R. Nolte, EPJ Web of Conferences **66**, 03077 (2014), France.
31. M.C. Lagunas-Solar, P.M. Kiefer, O.F. Carvacho, C.A. Lagunas, Y.P. Cha, Appl. Radiat. Isot. **42**, 643 (1991).
32. M.C. Lagunas-Solar, N.X. Zeng, I. Mirshad, T. Grey-Morgan, J. Am. Nucl. Soc. **74**, 137 (1996).
33. M.C. Lagunas-Solar, *Accelerator production of ^{99m}Tc with proton beams and enriched ^{100}Mo targets*, IAEA-TECDOC, Vol. **1065** (IAEA, Vienna, 1999) p. 87.
34. B. Scholten, R.M. Lambrecht, M. Cogneau, H. Vera Ruiz, Appl. Radiat. Isot. **51**, 69 (1999).
35. S. Takács, Z. Szucs, F. Tárkányi, A. Hermanne, M. Sonck, J. Radioanal. Nucl. Chem. **257**, 195 (2003).
36. M.S. Uddin, M. Hagiwara, F. Tarkanyi, F. Ditroi, M. Baba, Appl. Radiat. Isot. **60**, 911 (2004).
37. M.U. Khandaker, M.S. Uddin, K.S. Kim, Y.S. Lee, G.N. Kim, Nucl. Instrum. Methods Phys. Res. B **262**, 171 (2007).
38. M.U. Khandaker, M.S. Uddin, K.S. Kim, Y.S. Lee, G.N. Kim, Nucl. Instrum. Methods Phys. Res. B **264**, 201 (2007).
39. M.S. Uddin, M. Baba, Appl. Radiat. Isot. **66**, 208 (2008).
40. O. Lebeda, M. Pruszynski, Appl. Radiat. Isot. **68**, 2355 (2010).
41. K. Gagnon, F. Bénard, M. Kovacs, T.J. Ruth, P. Schaffer, J.S. Wilson, S.A. Mc Quarrie, Nucl. Med. Biol. **38**, 907 (2011).
42. F. Tárkányi, F. Ditrói, A. Hermanne, S. Takács, A.V. Ignatyuk, Nucl. Instrum. Methods Phys. Res. B **280**, 45 (2012).
43. W.F. Titus, Phys. Rev. **115**, 351 (1959).
44. R.W. Gellie, Aust. J. Phys. **21**, 765 (1968).
45. N. Mutsuro, Y. Ohnuki, K. Sato, M. Kimura, J. Phys. Soc. Jpn. **14**, 1649 (1959).
46. B.S. Ishkhanov, I.M. Kapitonov, E.V. Lazutin, I.M. Piskarev, O.P. Shevchenko, Yad. Fiz. **11**, 702 (1970) Sov. J. Nucl. Phys. **11**, 394 (1970).
47. H. Beil, R. Bergere, P. Carlos, A. Lepretre, A. De Miniac, A. Veyssiere, Nucl. Phys. A **227**, 427 (1974).
48. D. Habs, U. Köster, Appl. Phys. B **103**, 471 (2011).
49. H. Utsunomiya, S. Goriely, T. Kondo, C. Iwamoto, H. Akimune, T. Yamagata, H. Toyokawa, H. Harada, F. Kitatani, Y.W. Lui, A.C. Larsen, M. Guttormsen, P.E. Koehler, S. Hilaire, S. Peru, M. Martini, A.J. Koning, Phys. Rev. C **88**, 015805 (2013).
50. S.F. Mughabghab, M. Divadeenam, N.E. Holden, *Neutron resonance and thermal cross sections*, Vol. **I** (Academic Press, New York, 1981).
51. H. Naik, S.V. Suryanarayana, K.C. Jagadeesan, S.V. Thakare, P.V. Joshi, V.T. Nimje, K.C. Mittal, A. Goswami, V. Venugopal, S. Kailas, J. Radioanal. Nucl. Chem. **295**, 807 (2013).
52. Rita Crasta, H. Naik, S.V. Suryanarayana, P.M. Prajapati, K.C. Jagadisan, S.V. Thakare, S. Ganesh, V.T. Nimje, K.C. Mittal, A. Goswami, J. Radioanal. Nucl. Chem. **290**, 367 (2011).
53. H. Naik, G.N. Kim, R. Schwengner, K. Kim, M. Zaman, S.C. Yang, S.G. Shin, Y.-U. Kye, R. Massarczyk, R. John, A. Junghans, A. Wagner, A. Goswami, M.-H. Cho, Eur. Phys. J. A **52**, 47 (2016).
54. A.J. Koning, S. Hilaire, M.C. Duijvestijn, *TALYS: comprehensive nuclear reaction modeling*, in: *Proceedings of the International Conference on Nuclear Data for Science and Technology-ND 2004*, edited by R.C. Haight, M.B. Chadwick, T. Kawano, P. Talou, Vol. **769** (AIP, New York, 2005) pp. 1154–1159.
55. M. Erhard, A.R. Junghans, C. Nair, R. Schwengner, R. Beyer, J. Klug, K. Kosev, A. Wagner, Phys. Rev. C **81**, 034319 (2010).
56. R. Schwengner, R. Beyer, F. Donau, E. Gosse, A. Hartmann, A.R. Junghans, S. Mallian, G. Rusev, K.D. Schilling, W. Schulze, A. Wagner, Nucl. Instrum. Methods Phys. Res. A **555**, 211 (2005).
57. H. Naik, Sarbjit Singh, A. Goswami, V.K. Manchanda, G. Kim, K.S. Kim, M.W. Lee, Md. Shakilur Rahman, D. Raj, S. Ganesan, S.V. Suryanarayana, M.H. Cho, W. Namkung, Nucl. Instrum. Methods Phys. Res. B **269**, 1417 (2011).
58. C.F. Weizsacker, Z. Phys. **88**, 612 (1934).
59. E.J. Williams, Phys. Rev. **45**, 729 (1934).
60. GEANT4 Collaboration (S. Agostinelli *et al.*), Nucl. Instrum. Methods A **506**, 250 (2003).
61. B. Veyssiere, H. Beil, R. Bergere, P. Carlos, A. Lepretre, Nucl. Phys. A **159**, 561 (1970).
62. C. Fultz, R.L. Bramblett, J.T. Caldwell, N.A. Kerr, Phys. Rev. **127**, 1273 (1962).
63. K. Vogt, P. Mohr, M. Babilon, W. Bayer, D. Galaviz, T. Hartmann, C. Hutter, T. Rauscher, K. Sonnabend, S. Volz, A. Zilges, Nucl. Phys. A **707**, 241 (2002).
64. K.Y. Hara, H. Harada, F. Kitatani, S. Goko, S.Ya. Hohara, T. Kaihori, A. Makinaga, H. Utsunomiya, H. Toyokawa, K. Yamada, J. Nucl. Sci. Technol. **44**, 938 (2007).
65. V.V. Varlamov, B.S. Ishkhanov, V.N. Orlin, S.Yu. Troshchiev, Izv. Ross. Akad. Nauk Ser. Fiz. **74**, 884 (2010).
66. V.Di. Napoli, A.M. Lacerenja, F. Salvetti, H.G. De Carvalho, J. Benuzzi Martins, Lett. Nuovo Cimento **1**, 835 (1971).
67. O.A. Bezshyyko, A.N. Vodin, L.O. Golinka-Bezshyyko, A.M. Dovbnya, I.N. Kadenko, A.O. Kivernyk, A.A. Kovalenko, V.A. Kushnir, A.I. Levon, V.V. Mitrochenko, S.M. Olejnik, G.E. Tuller, Bull. Russ. Acad. Sci. Phys. **75**, 941 (2011).
68. A. Fessler, A.J.M. Plompen, D.L. Smith, J.W. Meadows, Y. Ikeda, Nucl. Sci. Eng. **134**, 171 (2000).
69. D.L. Smith, Nucl. Data Sheets **123**, 1 (2015).
70. DOE solicitation titled "molybdenum-99" DE-FOA-0000323, 29 Apr 2010.